Digital simulation of temperature and pressure effects in photoacoustic spectroscopy

Victor A. Fishman, and Allen J. Bard

Anal. Chem., **1980**, 52 (11), 1723-1729• DOI: 10.1021/ac50061a043 • Publication Date (Web): 01 May 2002

Digital Simulation of Temperature and Pressure Effects in Photoacoustic Spectroscopy

Victor A. Fishman and Allen J. Bard*

Department of Chemistry, The University of Texas at Austin, Austin, Texas 78712

A digital simulation method for treatment of the temperatures and pressures which arise in photoacoustic spectroscopy (PAS) with periodic and pulsed irradiation is described. Results obtained are shown to be in good agreement with those of earlier steady-state theoretical models and experimental measurements. The model allows observation of approach of the system to steady state and the inclusion of dissipation factors and sample variables.

The photoacoustic effect has been used since the 1940's to study relaxation phenomena in the gas phase (*1–3*). In 1973, experimental results were published (*4, 5*) demonstrating the qualitative similarity between the usual optical absorption and photoacoustic spectra of certain solid samples. A number of papers concerning the application of photoacoustic spectroscopy (PAS) to solids and strongly absorbing solutions have since appeared (see, for example (*6–10*) and recent reviews (*11–13*)).

In the PAS experiment, the sample is sealed in a small, fixed-volume, gas-filled cell containing a sensitive microphone as a detector. The sample is irradiated with high intensity, chopped monochromatic light through the cell window. The energy absorbed by the sample is converted to heat by radiationless transitions to lower lying energy states. This heat is transferred from the sample to the gas in the cell, generating a pressure wave in the fixed volume cell. This pressure wave is detected by the microphone. Alternatively, direct detection of the acoustic wave in the sample by a piezoelectric detector (PZT) attached directly to a bulk solid sample can be used (*14, 15*). The PZT has decided advantages when using microsecond pulsed radiation sources and/or samples with low surface area to volume ratios.

A number of recent papers dealing with the theory of the PAS effect have appeared (*16–22*). In all of these, the steady-state temperature and gas pressure fluctuations were obtained by assuming irradiation with sinusoidally modulated radiation and treating the diffusion of heat in the sample, gas, cell window, and sample backing material. The early work of Parker (*17*) treated the transfer of heat in the sample as a straightforward diffusion process. The acoustic coupling gas in the PAS cell was described using the more complete coupled diffusion and hydrodynamic equations. Parker initially concluded that the PAS signal was generated by a thin layer of molecules adsorbed on the cell window surface. Bennett and Forman (*18, 19*) also used thermal diffusion and linearized hydrodynamic equations to calculate the temperature profiles and the pressure amplitude in the acoustic coupling gas. Their work suggested experimental conditions under which a detectable acoustic pressure wave could be generated by bulk absorption in highly transparent laser glass. Parker's original work was later extended (*20*) to include cell geometry factors and the dissipative effects of the cell window. This extended treatment is especially useful for small cell volumes where the thermal diffusion length in the gas (μ_g) is greater than the total thickness of the gas (l_g).

McDonald and Wetsel (*21, 22*), in addition to using the more complete hydrodynamic treatment of the acoustic coupling gas, also considered the effect of generation of an acoustic wave in the sample. For the usual values of sample absorption coefficient (β, cm^{-1}) and sample thickness (l_s), this extended model agrees with the simpler approach of Rosencwaig and Gersho (*16*). This latter approach, which leads to an equation most easily applied to actual experimental measurements, treats the heat flow in all regions of the PAS system. Unlike the other treatments, which take into account the finite velocity of sound, Rosencwaig and Gersho calculated the temperature of the sample/gas interface and assumed an instantaneous pressure rise in the cell due to the action of an adiabatic acoustic piston adjacent to the sample surface. Even though this approach was less complex than the previous treatments, the equations that resulted were still rather complicated, but they could be simplified for certain limiting cases.

An alternate approach to the use of a periodically modulated (i.e., chopped) light source in PAS is the application of a pulsed source. The theory of this method, called time-domain PAS, has been described by Mandelis and Royce (*23*). These authors basically employed the same model as Rosencwaig and Gersho (*16*) and solved the heat conduction equations by the Laplace transform technique. Rather complicated equations result in Laplace space and inversion was only possible for special limiting cases. These authors considered the velocity of sound to be infinite and included loss of thermal energy via the cell window and backing material as the only dissipative mechanism.

This paper describes a digital simulation model for PAS based on the simplified thermal diffusion treatment of the system. The digital simulation does not depend on the steady-state assumption and provides information about the approach of the system from its initial condition to steady state. Moreover, it can be employed for any form of excitation, such as periodic (sinusoidal, square wave) or pulsed. The digital model also provides a convenient means of taking account of complicating effects, such as thermal dissipative effects thoughout the system (i.e., loss of heat to the sample backing material and through the cell walls and window), form of sample, and finite rates of heat transfer at the interfaces. The simulation provides a straightforward approach to a calculation of the effects of variation of the thermal, optical, and physical parameters of the system on the PAS signal. We show that these results agree well with previous theoretical treatments and experiments.

EXPERIMENTAL

The computer programs for the digital simulation were written in FORTRAN and require ~150K of memory in the CDC 6400/6600 system.

The basic PAS spectrometer operating in the single beam mode has been described elsewhere (*8*). The sample cell (Figure 1) was machined from aluminum and employed O-ring seals. The differential output from the 1-inch ceramic microphone (General Radio 1560-9065, −61.6 db re 1 V/μbar) fed directly to a dual channel lock-in amplifier (Princeton Applied Research Model

0003-2700/80/0352-1723$01.00/0

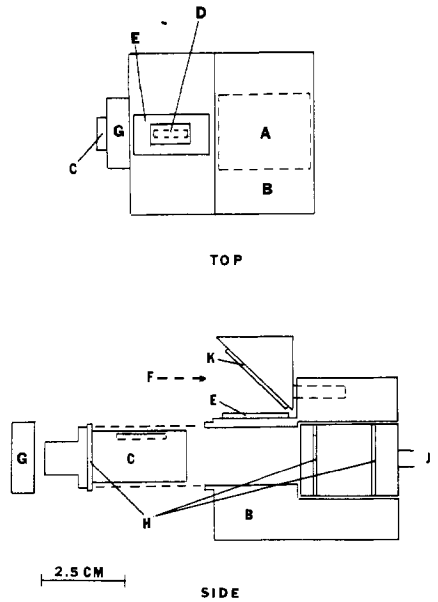

Figure 1. Aluminum PAS cell: (a) microphone, (b) aluminum cell body, (c) sample holder, (d) sample boat, (e) quartz window, (f) incident radiation, (g) threaded ring, (h) O-ring seals, (j) microphone leads, (k) front surface mirror

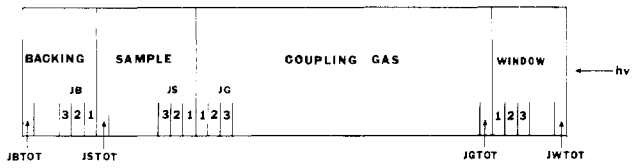

Figure 2. One-dimensional model of the PAS system

5204). The analog output from the lock-in amplifier was digitized and recorded on a Bascom-Turner model 8110 electronic recorder.

Optical absorption spectra were obtained with a Cary Model 14 spectrophotometer. Spectra of highly absorbing samples were obtained using cells constructed from thin Teflon spacers (0.5 to 3 mil) between optically flat glass plates.

Methylene blue dye (Fisher reagent grade, total dye content 89.2%) dissolved in distilled water was used to prepare sample solutions. Solution samples (volume, 150 μL) filled the sample cup to a depth of approximately 3 mm.

SIMULATION MODEL

Digital simulation techniques have been applied to numerous electrochemical problems, such as rotating ring-disk electrodes (*24*), electrogenerated chemiluminescence (*25*), and semiconductor electrodes (*26*). An in-depth discussion of the use of digital simulation in electrode processes can be found in the review by Feldberg (*27*). The similarity of the partial differential equations for diffusion and heat conduction allows straightforward application of the techniques employed in electrochemistry to PAS. Thus the heat conduction equations are written in finite difference form. The cell space is divided into finite elements of width, Δx, as shown in Figure 2, and the time period of interest into elements of duration, Δt. The accuracy of finite-difference methods increases as the magnitude of the discrete intervals of interest decreases. The simulation parameters are selected to produce results which represent a compromise between accuracy and computational time. In performing the digital computation, the simulation variables and equations are expressed in dimensionless form to allow the results to apply to a wide variety of experimental conditions.

Consider the 1-dimensional model shown in Figure 2. The linear distance in each region is divided into segments, indexed by the letter J, with $JiTOT = li/\Delta x_i$, where the subscript and index i indicate the appropriate region, li(cm) is the total length of region i, Δx_i(cm) is the size of the space interval and $JiTOT$ is the total number of space intervals in that region. The subscript and index i will be either S (sample), B (backing), G (gas), or W (window).

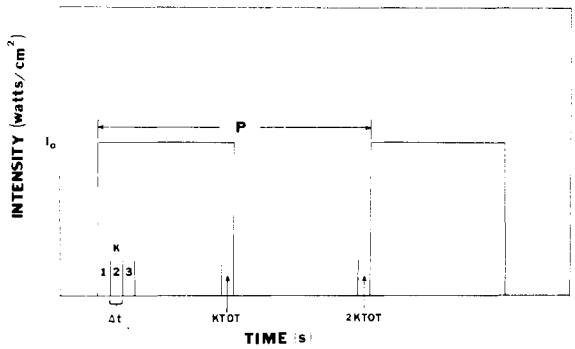

Figure 3. Intensity vs. time plot for square wave chopped incident light showing time interval Δt

The square wave chopped monochromatic light source is represented in the intensity vs. time plot of Figure 3. The chopping period is divided into 2KTOT equal time intervals, indexed by the letter K, with the size of each interval being Δt(s) = Period/2KTOT.

Figure 4 shows a flow chart of the program model. Each of the program sections is discussed below.

Initial Conditions. Prior to the first light pulse, the entire system is at the ambient temperature. This is written as $Ti(Ji) = T_a$, where $Ti(Ji)$ is the temperature at the midpoint of the space interval J in the region i and T_a is the ambient temperature. $Ti(Ji)$ is converted to a dimensionless fractional temperature parameter by dividing it by T_a. Thus, prior to the first light pulse

$$FTi(Ji) = Ti(Ji)/T_a = 1 \tag{1}$$

where $FTi(Ji)$ is the dimensionless fractional temperature. The time index, K, is 0, at $t = 0$.

Absorption of Light and Generation of Initial Temperature Gradients. A homogeneous, isotropic sample whose optical absorption properties can be described by the Beer–Lambert law is assumed.

$$I_x = I_0 e^{-\beta x} \tag{2}$$

where I_x = intensity at the point x (watts/cm^2); I_0 = light intensity at the sample surface; β = absorptivity or absorption coefficient of the transition (cm^{-1}); x = perpendicular distance from the sample surface (cm). For very small changes in x, Equation 2 can be differentiated to give

$$\frac{dI_x}{dx} = -\beta I_0 e^{-\beta x} \tag{3}$$

which can be written directly in finite difference form

$$\Delta I_x = -\beta I_0 e^{-\beta x}\, \Delta x \tag{4}$$

This linearized approximation agrees to within 5% of the exact form when $\beta \Delta x/2 < 0.3$.

The light absorption (ΔI_x) and the resulting radiationless de-excitation will cause the temperature in the space interval Δx to rise. This temperature variance ΔT_x is proportional to the total power absorbed by the sample, $P_{abs} = \Delta I_x \cdot A$, and is given by

$$\Delta T_x(°C) = \frac{(0.239) P_{abs} \eta\, \Delta t}{\rho C_p A \Delta X} \tag{5}$$

where (0.239) converts watts to cal/s, η is the efficiency of absorbed light to heat conversion, ρ is the sample density

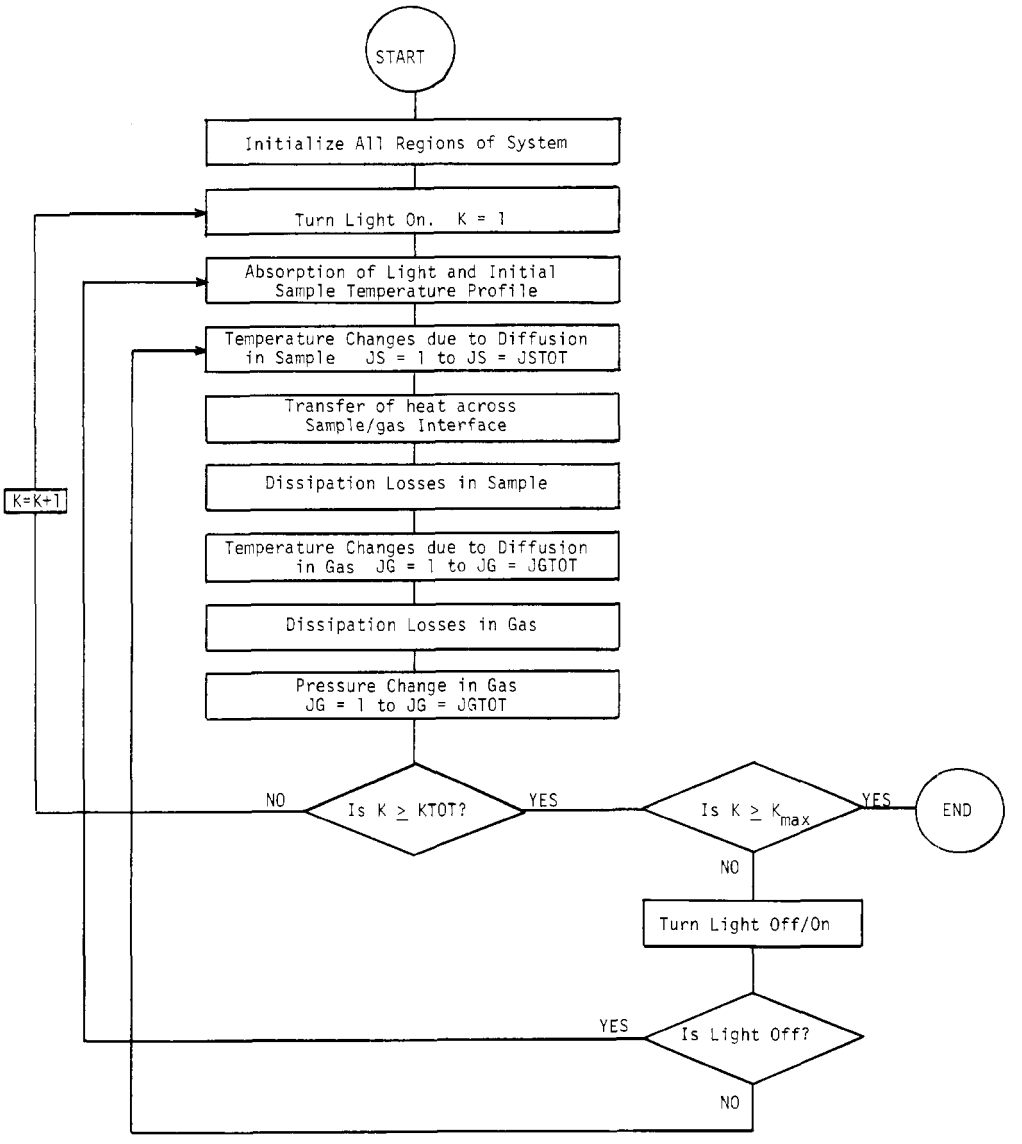

Figure 4. Block diagram of program model

(g/cm^3), C_p is the sample specific heat at constant pressure (cal/g °C), and A is the illuminated surface area of sample (cm^2). η was assumed to be unity in most cases, i.e., photoreaction or photoemission processes do not occur. The temperature increase ΔT_x is connected to ΔFT_x by dividing by T_a. This allows ΔFT_x to be written in terms of the dimensionless simulation parameter *RINT* and the exponential term of the optical absorption

$$\Delta FT_x = RINT\, e^{-\beta x} \tag{6}$$

$$RINT = \frac{0.239\, I_0 \beta\, \Delta t}{\rho_s C_p T_a} \tag{7}$$

Thermal Diffusion in the Bulk Phase. Bulk phase conduction processes for isotropic homogeneous media are described by the heat diffusion equation

$$\frac{\partial Ti}{\partial t} = \alpha_i \frac{\partial^2 Ti}{\partial x_i^2} \tag{8}$$

The parameter α_i is the thermal diffusivity, $\alpha_i = k_i/\rho_i C_{pi}$ (cm^2/s), where k_i is the thermal conductivity in region i (cal/s cm °C). Equation 8 applies to all regions. The usual distributed heat source term in the equation for the absorbing sample has already been considered by equation 6.

Equation 8 is converted to finite-difference form by using the central-difference approximation for the second derivative (*28*)

$$\frac{\Delta Ti(J)}{\Delta t} = \frac{\alpha_i}{(\Delta x)^2}\,[Ti(J+1) - 2Ti(J) + Ti(J-1)] \tag{9}$$

Conversion of Equation 8 to the fractional dimensionless form yields the simulation parameter *ALPHi*

$$\Delta FTi(J) = ALPHi[FTi(J+1) - 2FTi(J) + FTi(J-1)] \tag{10}$$

$$ALPHi = \frac{\alpha_i \Delta t}{(\Delta x_i)^2} \tag{11}$$

$\Delta FTi(J)$ is the fractional dimensionless temperature change due to diffusion in the coordinate interval J of region i.

Transfer of Heat across an Interface. Heat transfer across an interface requires consideration of the heat flux:

$$\text{Heat flux} = k_i \frac{\partial T}{\partial x} \tag{12}$$

In finite difference format, this becomes

$$\Delta FTi(J=1) = ALPHi[FTi(J=1) - FTi(J=2)] \tag{13}$$

The boundary conditions for the continuity of temperature and heat flux at the interface are

$$T_0 = Ti(Ji = 0) = Ti'(Ji' = 0) \quad (14)$$

and

$$k_i\left(\frac{\partial T}{\partial x}\right)_{x=0} = k_{i'}\left(\frac{\partial T}{\partial x}\right)_{x=0} \quad (15)$$

where T_0 is the temperature at the interface.

As before the finite difference form of Equation 15 is

$$\frac{k_i}{\frac{1}{2}\Delta x_i}[T_0 - Ti(Ji = 0)] = \frac{k_{i'}}{\frac{1}{2}\Delta x_{i'}}[Ti'(Ji' = 0) - T_0] \quad (16)$$

Equations 14 and 16 can be solved for T_0 in terms of the temperatures in the first space intervals of the adjacent regions i and i'.

$$T_0 = \left[\frac{1}{\frac{k_i}{\Delta x_i} + \frac{k_{i'}}{\Delta x_{i'}}}\right]\left[\left(\frac{k_{i'}}{\Delta x_{i'}}\right)Ti'(Ji' = 1) + \left(\frac{k_i}{\Delta x_i}\right)Ti(Ji = 1)\right] \quad (17)$$

The heat flux at the interface is found by substitution of Equation 17 into Equation 16.

$$\text{heat flux} = H[Ti'(Ji' = 1) - Ti(Ji = 1)] \quad (18)$$

$$H = \frac{\left(\frac{k_{i'}}{\Delta x_{i'}}\right)\left(\frac{k_i}{\Delta x_i}\right)}{\left(\frac{k_{i'}}{\Delta x_{i'}}\right)\left(\frac{k_i}{\Delta x_i}\right)} \quad (19)$$

Equation 18 is the condition for linear heat transfer across an interface. The simulation parameter H is the coefficient of surface heat transfer (*29*).

The heat flux at the interface causes a temperature change in the first space interval of the adjacent regions i and i'. With the appropriate conversion factors, this temperature change can be written as

$$\Delta FTi(Ji = 1) = RFLUXi\,[FTi'(Ji' = 1) - FTi(Ji = 1)] \quad (20)$$

$$RFLUXi = \frac{H\,\Delta t}{C_i\rho_i\Delta x_i} \quad (21)$$

An analogous equation holds for region i'.

Examination of the previous sections shows that at a given instant of time, K, the change in the temperature of any space element is obtained by summing the changes due to light absorption and thermal diffusion. This summation is thus added to the existing temperature profile, $(FTi(Ji,K - 1))$.

Pressure Change in the Coupling Gas. The pressure wave in the acoustic coupling gas is assumed to arise from an adiabatic compression resulting from the change in volume in the space intervals (Ji) due to the temperature changes in those intervals. The explicit assumption of an acoustic piston (*16*) is not required. For the adiabatic expansion of an ideal gas $PV^\gamma = \text{const}$, $\gamma = C_p/C_v = 1.4$ (air). Differentiation of this expression yields

$$\frac{dP}{P_a} = -\gamma\,dV/V_0 \quad (22)$$

where dP is the excess pressure, P_a is the ambient pressure (bar), and V_0 is the volume of gas (cm^3). Note that the quotient (dP/P_a) represents a dimensionless fractional pressure (FP). The volume change in the space element (JG) of the gas is

$$\Delta V(JG) = 0.00367\,V(JG)\,\Delta T(JG) \quad (23)$$

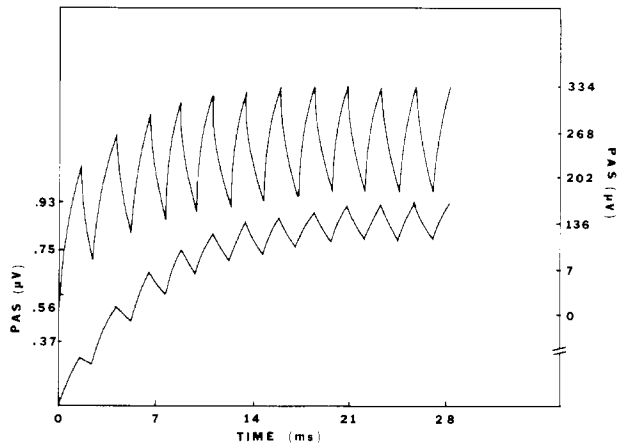

Figure 5. Digital simulation of PAS signal for aqueous absorbing sample. Lower trace: $\beta = 1$ relates to left hand axis. Upper trace: $\beta = 500$ relates to right hand axis. Chopping frequency, $f = 400$ Hz

where 0.00367 is the coefficient of expansion per unit increase in temperature for an ideal gas and $V(JG)$ is the volume of the space element (JG). Combination of Equations 22 and 23 yields the fractional pressure in the space element (JG),

$$FP(JG) = \frac{-\gamma(0.00367)\,V(JG)\,\Delta TG(JG)}{V_0} \quad (24)$$

In the dimensionless finite-difference form, Equation 24 is

$$FP(JG) = \frac{-(0.00367)\gamma T_a\,\Delta FTG(JG)}{JGTOT} \quad (25)$$

The total pressure change in the acoustic coupling gas is found by summing over the temperature changes in all of the space elements (JG). Thus, during a given time interval K, the total pressure change is

$$FP(K) = \frac{-(0.00367)\gamma T_a}{JGTOT}\sum_{JG=1}^{JGTOT}\Delta FTG(JG) \quad (26)$$

In practice, the upper limit of the summation over the space elements in the gas need only include those elements that have a significant value of $\Delta FTG(JG)$, i.e., respond to the cyclic heating and cooling of the gas. This region (of thickness $\sim 2\pi\mu_g$) is analagous to the acoustic piston of Rosencwaig and Gersho (*16*) and develops naturally from the calculations.

RESULTS

The thermal diffusion length in the gas (μ_g) at a given chopping frequency is determined in the simulation by calculating the steady-state temperature profile in the gas and noting the linear distance from the sample/gas interface for the gas temperature to decrease by 90% of its value at the sample surface. The variation of μ_g with $f^{-1/2}$ thus calculated is linear (correlation coefficient = 0.996) and exactly coincident with that generated by application of the Rosencwaig-Gersho theory.

The time-dependent photoacoustic signal for two values of β as predicted by the digital simulation is plotted in Figure 5. The exciting radiation is square-wave modulated and the sample is an absorbing aqueous solution. The upper and lower trace are for $\beta = 1$ cm^{-1} and $\beta = 500$ cm^{-1}, respectively, at $f = 400$ Hz. The steady state as indicated by no further change in the peak-to-peak magnitude of the PAS signal is obtained in 11 cycles.

The model was used to simulate the variation of PAS signal with variation in sample absorption coefficient. The results are shown in Figure 6. At small values of β (<100 cm^{-1}), the PAS signal is directly proportional to β. The onset of thermal saturation removes this linearity, eventually leading to a region

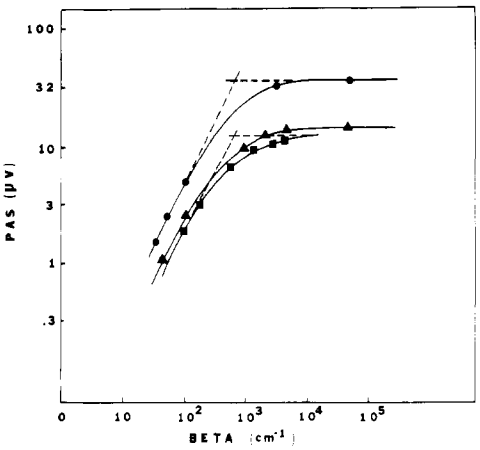

Figure 6. Log–log plot of PAS signal vs. β for methylene blue dye solutions: (●-●-●) simulation, (▲-▲-▲) simulation including dissipation, (■-■-■) experimental. Chopping frequency, f = 100 Hz, β_c = 658 cm^{-1}

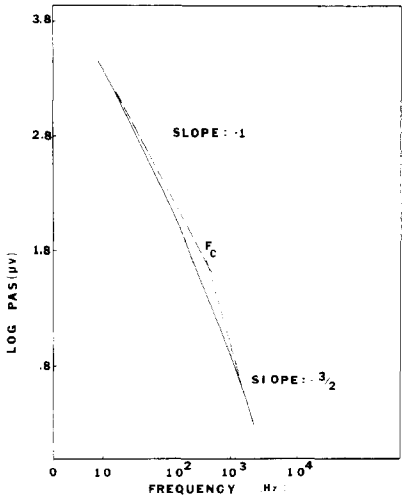

Figure 7. Simulation generated log–log plot of PAS signal vs. frequency for GaP single crystal. β = 200 cm^{-1}, at λ = 522 nm

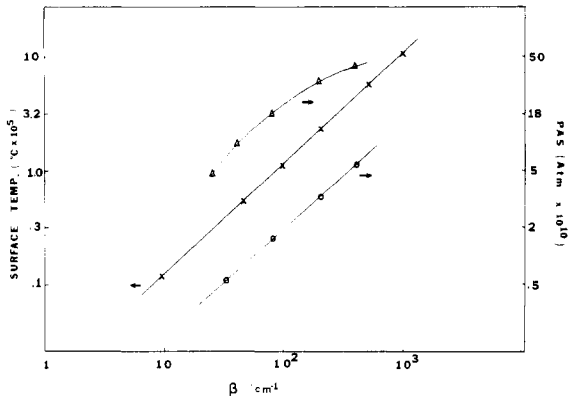

Figure 8. Simulated pulse-PAS experiment: (X-X-X) sample surface temperature vs. β (left hand axis), PAS signal vs. β (right hand axis). (O-O-O) ~0.2 ms after pulse; (Δ-Δ-Δ) 0.8 ms after pulse.

of total thermal saturation where the PAS signal shows no β dependence ($\sim\beta > 5 \times 10^4$ cm^{-1}). For the system modeled in Figure 6, the sample is an absorbing aqueous solution at a chopping frequency of 100 Hz.

The variation of the PAS signal with frequency for single crystal GaP was simulated and the results are plotted in Figure 7. The plot shows a slope of −1 at low frequencies, decreasing to −3/2 at higher frequencies. The absorption coefficient of β = 200 cm^{-1} corresponds to the absorption of GaP at λ = 522 nm.

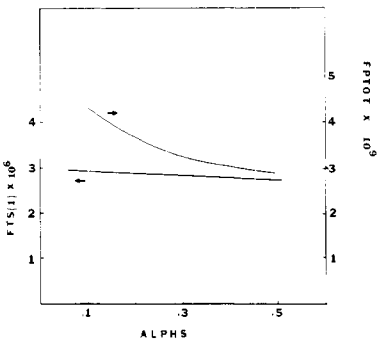

Figure 9. Simulated pulse PAS experiment indicating variation of surface temperature and pressure with variation in sample thermal parameter, *ALPHS*, for an absorbing aqueous solution, β = 500 cm^{-1}

Table I. Correspondence between Simulation and Experimental Parameters

simulation dimensionless parameter	experimental parameter and usual units
K	Δt, s
Ji	Δx, cm
ALPHi	α, cm^2/s
RFLUXi	k, cal/s, cm °C
RINT	I_0, cal/s

Table II. Typical Thermal Constants

material	k, cal/s cm °C	ρ, g/cm^3	c, cal/g °C
H_2O	1.43×10^{-3}	1.0	1.0
air	6×10^{-5}	1.18×10^{-3}	0.248
GaP	2.0×10^{-2}	4.13	0.202

The results of the simulation of the PAS experiment with pulsed light excitation are shown in Figure 8. The excitation was taken to be a 5.5-μs pulse and the sample an absorbing aqueous solution. The sample surface temperature and the cell pressure at 200 μs and 800 μs are plotted against the absorption coefficient β. The sample surface temperature is linear with β over the entire range $10 < \beta < 10^3$ cm^{-1}. The cell pressure at 800 μs after the pulse, by contrast, shows no linearity with β over the region modeled.

The simulated variation of the sample surface temperature and cell pressure with variation in sample thermal properties (ALPHS) for the pulsed PAS experiment are shown in Figure 9. The sample surface temperature shows very little dependence on *ALPHS* whereas the cell pressure shows a marked *ALPHS* dependence that decreases as *ALPHS* increases.

DISCUSSION

The digital simulation variables and their equivalent experimental parameters are shown in Table I and the thermal and physical parameters for water, GaP, and air are listed in Table II. In simulations of a solution sample, the thermal and physical properties of the sample were taken to be those of the solvent with the sample optical properties governed by the absorbance of the solution. Computational efficiency requires that *ALPHi* be as large as possible. The nature of the finite difference formulation places an upper limit on *ALPHi* of 0.5. It is convenient to take *ALPHi* = 0.45 (*27*). This constraint fixes the value of the quotient, $\alpha_i/(\Delta x_i)^2$, for all regions of the system.

The use of the sample/gas PAS system requires that the acoustic coupling gas transmit the heat absorbed by the sample to the microphone detector in the form of a pressure pulse. The a priori inclusion by Rosencwaig and Gersho (*16*) of the acoustic piston construct is justified by the simulation

results noted in the Results section. The equation describing the thermal diffusion length in the gas used by Rosencwaig and Gersho is $\mu_g = 2((\pi f/\alpha_g))^{-1/2}$. Thus the predicted plot of log μ_g vs. log $f^{-1/2}$ is linear with slope −1.

Before comparing further simulation and experimental results, it is useful to develop the concept of critical parameters to describe the PAS experiment. Rosencwaig and Gersho (*16*) derived explicit expressions specifying the pressure variation in the gas. This yields the expression for the PAS signal, Q, also used by Wetsel and McDonald (*22*) for optically opaque ($1/\beta \ll l_s$) and thermally thick ($\mu_s \ll l_s$) samples:

$$Q = \left[\frac{\beta I_0 \gamma P_a}{2\sqrt{2}k_s l_g a_g T_a}\right]\left[\frac{(r-1)}{(g+1)(\beta^2 - b_s^2)}\right] \quad (27)$$

where $r = (1-j)\beta/2a_s$, $a_s = (\pi f/\alpha_s)^{1/2}$, $g = (k_s/k_g)(\alpha_s/\alpha_g)^{1/2}$, and $b_s = (1+j)\,a_s$. A constant, R, independent of frequency, f, and absorption coefficient can be defined such that

$$Q' = Q/R = \beta(r-1)/[a_g(\beta^2 - b_s^2)] \quad (28)$$

where

$$R = \frac{\gamma I_0 P_a}{2\sqrt{2}k_s l_g T_a(g+1)} \quad (29)$$

When $\beta \ll b_s$ (the nonsaturated region), Equation 28 can be approximated as

$$\log |Q| = -3/2 \log (2\pi f) + 1/2 \log (2\alpha_g \alpha_s^2 \beta^2) \quad (30)$$

When $\beta \gg b_s$ (the saturated region), Equation 28 yields

$$\log |Q| = -\log (2\pi f) + 1/2 \log (1/2\alpha_s \alpha_g) \quad (31)$$

The values of β and f for which Equations 30 and 31 have a common solution will be defined as the critical values, β_c and f_c, respectively. Thus

$$f_c = (\alpha_s/2\pi)\beta_c^2 \quad (32)$$

In the PAS experiment in which the signal is recorded as a function of chopping frequency, extrapolation of the two limiting regions described by Equations 30 and 31 to their point of intersection will yield a value for f_c corresponding to Equation 32. Similarly, in the PAS signal vs. absorption coefficient experiment, at a given chopping frequency, extrapolation of the region where the signal linearly increases with an increase in β to intersect with the extrapolation of the saturation region where the signal is independent of β yields a value of β_c corresponding to Equation 32.

The limiting behavior and the determination of β_c and f_c for a typical PAS experiment are shown in Figures 6 and 7, respectively. These critical parameters are less ambiguous than the concepts of "onset" and "total" saturation sometimes employed in describing PAS results.

McClelland and Kniseley (*7*) studied the variation of the PAS signal of aqueous methylene blue dye solutions of different concentration. With the thermal parameters of the solvent, Equation 32 yields a theoretical value of $\beta_c = 658$ cm^{-1} at $f = 100$ Hz. Comparison of the experiments done in this laboratory and the simulation results, assuming no dissipation of heat from the system, is shown in Figure 6. This comparison can be used to estimate the overall efficiency of the PAS system. The theoretical curve shown in Figure 6 represents the maximum PAS signal possible given the particular thermal, physical, and geometrical properties of the simulated system. Any effects that operate to dissipate the heat in the system will reduce the magnitude of the PAS signal. In the case shown in Figure 6, the experimental signal level was approximately 37% of the theoretical maximum.

In addition to the effects described in the previous sections, the simulation of PAS requires taking account of the thermal dissipation of heat out of the cell. This can occur through

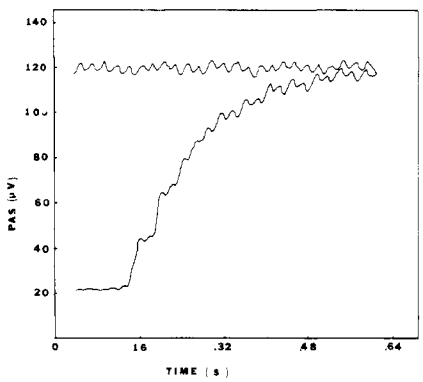

Figure 10. Experimentally observed in-phase PAS signal of polished aluminum sample. High intensity white light radiation chopped at 25 Hz

the sample backing material, cell walls, and window and will depend on the sample type (powder, gel, liquid), acoustic coupling gas, and cell material and geometry. Neither the exact contribution of these separate factors nor their effect on each other can be determined easily. However, it is possible to lump together the dissipative effects in each region of the system (sample, backing material, etc.) to yield a net dissipation factor for each region. In the digital simulation model the real time dissipative effects were calculated by multiplying the temperature in a given space interval at a given time by a dissipation factor for that region. Thus,

$$FTi(Ji,K) = FTi(Ji,K) \times DISFi \quad (33)$$

where $DISFi$, the dissipation factor for the region i, is a number ≤ 1. For the PAS cell described in Figure 2 and the simulation work cited in this paper, the dissipation factors were taken as $DISFS = 0.998$ and $DISFG = 0.95$; these values gave simulated behavior which approximated the experimental results. For highly absorbing thin film samples and PAS cells where the distance between the sample and the cell window is of the order of μ_g, the dissipation factors for the sample backing material and the cell window must also be included. The experimental approach to the steady state for a sample with very low β (polished aluminum) with high intensity white light irradiation at $f = 25$ Hz is shown in Figure 10. Comparison with the simulation results of Figure 5 shows the marked similarity.

If only dissipation to the sample backing material and cell window were considered, the simulation would indicate that attainment of the steady state would require 270 cycles ($f = 400$ Hz) and the increase in the initial PAS signal with time would be linear, showing no cyclical behavior during about the first 30 cycles. The time required to reach steady state depends strongly on the amount of heat dissipation in the sample as opposed to dissipation of the thermal wave in the gas. Further, dissipative effects cause the signal magnitude at steady state to be ~59% of that when no dissipative effects are considered.

This figure compares well with the experimental result of 37% previously noted in Figure 6. The addition of the dissipation factors greatly improves the fit between experimental and simulation results as shown in Figure 6.

A PAS experiment with a GaP single crystal has been reported by Rosencwaig (*30, 31*). Examination of Rosencwaig's data (*30*) yields an experimental value of $f_c \cong 300$ Hz at $\lambda = 522$ nm. This compares well with the value calculated by Equation 32, $f_c = 318$ Hz. The simulated frequency domain experiment for the GaP/air system shown in Figure 7 yields an extrapolated value of about 318 Hz. Although extrapolation of the log signal vs. log frequency plot involves some uncertainty, the simulation result agrees quite well with the experimental one. The determination of the critical values, β_c

and f_c, in principal allows separation of the optical and thermal properties of the sample. In practice, experimentally achieving the high frequency, nonsaturation region where the log–log plot of PAS signal vs. frequency has a $-3/2$ slope is difficult because the signal level is decreasing in this region. Also, variation of the sample absorption coefficient (β) is not possible with most types of samples. Thus, the important goal in PAS of obtaining β independent of the sample thermal properties has yet to be realized.

However, preliminary results of simulated pulsed PAS experiments indicate that the possibility for observation of sample optical properties independent of sample thermal properties and sample thickness exists with short pulses. In this case, fast transient signal averaging instruments (rather than lock-in amplifiers) are required to detect the signal due to instantaneous heat transfer from the illuminated surface of the sample. The results of the simulation of the pulsed-PAS experiment shown in Figure 8, as previously noted, show that the surface temperature is proportional to β even after the sample becomes transparent ($\beta < 100$ cm^{-1}). The effects of thermal diffusion can be seen in the complete loss of direct proportionality with β of the cell pressure at 800 μs after the pulse. This suggests that detection of the surface temperature immediately after the pulse but prior to significant thermal diffusion in the sample is warranted. Further, support for this approach is indicated by the results plotted in Figure 9. Hence, the sample surface temperature is shown to be independent of the sample thermal properties (*ALPHS*) in the pulsed-PAS experiment. In contrast, the cell pressure at 800 μs after the pulse shows a definite dependence on *ALPHS*.

Fast detection of the thermal energy at the illuminated face of the sample is approached most directly using the gas/microphone system where the volume of the acoustic coupling gas is minimized.

The use of PZT detection, while having the advantage of high sensitivity and relatively fast response times will give a response directly proportional to β only for thin films where the total absorbed power will be proportional to β. For samples with very low transmission coefficients, the total absorbed power will be β-independent and only intensity limited. Since the PZT will respond to the total absorbed power, no β-dependent signal is possible.

Recent work by Patel and Tam (*32*) using a microsecond pulsed laser to investigate weak absorptions in benzene using piezoelectric detection (PZT) indicates that the effects of thermal diffusion can be neglected in the microsecond pulse experiment. Clearly, the precise simulation of the pulsed PAS experiment will require the inclusion of the finite velocity of sound. Further, as noted by Wetsel and McDonald (*22*) and by McDonald (*33*), the PAS measurement may be affected by thermally generated mechanical motion of the sample. The extent of the contribution of these thermoacoustically generated elastic waves will depend on the optical absorption properties and thermal expansion coefficient of the sample. McDonald's results indicate that the thermoacoustic effect should be included in the photoacoustic determination of small ($\beta \leq 10^{-2}$ cm^{-1}) absorption coefficients.

Modification of the digital simulation to include the thermoacoustic effect due to the thermal expansion of the sample indicated no significant changes in the PAS signal for $\beta \geq 10$ cm^{-1} and chopping frequency $f \leq 1600$ Hz.

Viscosity effects in the acoustic coupling gas can usually be neglected since their contribution is significant only when the diameter of the smallest gas channel in the cell is on the order of $d \sim 0.1$ mm (air) (*31*).

CONCLUSIONS

The digital simulation model of the PAS effect can be applied to a variety of experiments. It is useful in the description of transient as well as steady-state phenomena. An accurate estimation of the relative efficiency of a particular experimental arrangement can be made through the investigation of the real time dissipative effects in the system. The simulation indicates that pulse-PAS experiments should provide a means of separation of sample thermal and optical properties. Experiments attempting to verify this are under way.

ACKNOWLEDGMENT

The authors thank Steve Feldberg for helpful discussions and R. C. Gray for assistance in construction of the PAS cell.

LITERATURE CITED

(1) Luft, K. F. *J. Tech. Phys.* **1943**, *24*, 97.
(2) Veingerov, M. L. *Dokl. Akad. Nauk. USSR* **1945**, *46*, 182.
(3) De Groot, M. S.; Emeis, C. A.; Hesselman, I. A. M.; Dreut, E.; Farenhorst, E. *Chem. Phys. Lett.* **1972**, *17*, 352.
(4) Harshbarger, W. R.; Robin, M. B. *Acc. Chem. Res.* **1973**, *6*, 329.
(5) Rosencwaig, A. *Opt. Commun.* **1973**, *7*, 305.
(6) McClelland, J. F.; Kniseley, R. N. *Appl. Opt.* **1976**, *15*, 2967.
(7) McClelland, J. F.; Kniseley, R. N. *Appl. Phys. Lett.* **1976**, *28*(8), 467.
(8) Gray, R. C.; Fishman, V. A.; Bard, A. J. *Anal. Chem.* **1977**, *49*, 697.
(9) Adams, M. J.; King, A. A.; Kirkbright, G. F. *Analyst (London)* **1976**, *101*, 73, 553.
(10) Adams, M. J.; Kirkbright, G. F. *Spectrosc. Lett.* **1976**, *9*(5), 255.
(11) Rosencwaig, A. *Phys. Today* **1975**, *28*, 23.
(12) Rosencwaig, A. *Anal. Chem.* **1975**, *47*, 592A.
(13) "Optoacoustic Spectroscopy and Detection", Pae, Yoh-Han, Ed.; Academic Press: New York, 1977.
(14) Eyring, E. M.; Farrow, M. M.; Burnham, R. K.; Azanneau, M. A.; Olsen, S. L.; Purdie, N. *Appl. Opt.* **1978**, *17*, 1093.
(15) Malpas, R. E.; Bard, A. J. *Anal. Chem.* **1980**, *52*, 109.
(16) Rosencwaig, A.; Gersho, A. J. *Appl. Phys.* **1976**, *47*, 64.
(17) Parker, J. G. *Appl. Opt.* **1973**, *12*(12), 2974.
(18) Bennett, H. S.; Forman, R. A. *Appl. Opt.* **1976**, *15*(5), 1313.
(19) Bennett, H. S.; Forman, R. A. *J. Appl. Phys.* **1977**, *48*(4), 1432.
(20) Aamodt, L. C.; Murphy, J. C.; Parker, J. G. *J. Appl. Phys.* **1977**, *48*, 927.
(21) McDonald, F. A.; Wetsel, G. C., Jr. *J. Appl. Phys.* **1978**, *49*, 2313.
(22) Wetsel, G. C., Jr.; McDonald, F. A. *Appl. Phys. Lett.* **1977**, *30*(5), 252.
(23) Mandelis, A.; Royce, B.S.H. *J. Appl. Phys.* **1979**, *50*(6), 4330.
(24) Prater, K. B.; Bard, A. J. *J. Electrochem. Soc.* **1970**, *117*(2), 207.
(25) Maloy, J. T.; Prater, K. B.; Bard, A. J. *J. Am. Chem. Soc.* **1971**, *93*, 5959.
(26) Laser, D.; Bard, A. J. *J. Electrochem. Soc.* **1976**, *123*(12), 1833.
(27) Feldberg, S. W. "Electroanalytical Chemistry", Volume 3, Bard, A. J., Ed.; Marcel Dekker, New York, 1969; Chapter 2.
(28) Chapman, A. J. "Heat Transfer", Macmillan and Co.: New York, 1967; Chapter 5.
(29) Carslaw, H. S.; Jaeger, J. C. "Conduction of Heat in Solids"; Oxford at Clarendon: London, 1959; p 19.
(30) Rosencwaig, A. *Rev. Sci. Instrum.* **1977**, *48*(9), 1133.
(31) Rosencwaig, A. *J. Appl. Phys.* **1978**, *49*(5), 2905.
(32) Patel, C. K. N.; Tam, A. C. *Appl. Phys. Lett.* **1979**, *34*(7), 467.
(33) McDonald, F. A. *Appl. Opt.* **1979**, *18*(9), 1363.

RECEIVED for review February 25, 1980. Accepted June 9, 1980. The support of this work by the National Science Foundation and the Robert A. Welch Foundation is gratefully acknowledged.